

# Bifurcation parameters of a reflected shock wave in cylindrical channels of different roughnesses

O. Penyazkov<sup>1</sup> · A. Skilandz<sup>1</sup>

Received: 6 November 2015 / Revised: 27 June 2017 / Accepted: 28 June 2017 / Published online: 24 July 2017  
© Springer-Verlag GmbH Germany 2017

**Abstract** To investigate the effect of bifurcation on the induction time in cylindrical shock tubes used for chemical kinetic experiments, one should know the parameters of the bifurcation structure of a reflected shock wave. The dynamics and parameters of the shock wave bifurcation, which are caused by reflected shock wave–boundary layer interactions, are studied experimentally in argon, in air, and in a hydrogen–nitrogen mixture for Mach numbers  $M = 1.3$ – $3.5$  in a 76-mm-diameter shock tube without any ramp. Measurements were taken at a constant gas density behind the reflected shock wave. Over a wide range of experimental conditions, we studied the axial projection of the oblique shock wave and the pressure distribution in the vicinity of the triple Mach configuration at 50, 150, and 250 mm from the endwall, using side-wall schlieren and pressure measurements. Experiments on a polished shock tube and a shock tube with a surface roughness of  $20\ \mu\text{m Ra}$  were carried out. The surface roughness was used for initiating small-scale turbulence in the boundary layer behind the incident shock wave. The effect of small-scale turbulence on the homogenization of the transition zone from the laminar to turbulent boundary layer along the shock tube perimeter was assessed, assuming its influence on a subsequent stabilization of the bifurcation structure size versus incident shock wave Mach number, as well as local flow parameters behind the reflected shock wave. The influence of surface roughness on the bifurcation development and pressure fluctuations near the wall, as well as on the Mach number, at which the bifurcation first

develops, was analyzed. It was found that even small additional surface roughness can lead to an overshoot in pressure growth by a factor of two, but it can stabilize the bifurcation structure along the shock tube perimeter.

**Keywords** Bifurcation of reflected shock wave · Surface roughness · Flow stabilization · Overshoot pressure · Small-scale turbulence

## 1 Introduction

Often, researchers encounter bifurcation phenomena when solving problems on supersonic flow around different obstacles such as supersonic air intakes, transonic wings, etc. The results of the previous reflected shock wave (RSW) bifurcation studies were analyzed in [1]. There are many contradictory assumptions concerning bifurcation formation in unsteady-state regimes and when the intensity of an incident shock wave (ISW) is changed. Up to now, most of the researchers dealing with RSW bifurcation adopted the simple model proposed by Mark [2] in 1958.

In shock tube experiments on monoatomic gases at low Mach numbers, during the wave travelling the reflected shock wave–boundary layer interaction causes the wave front to curve near the tube wall. A quasi-steady shape of the front is attained at some distance equal to several tube diameters [3]. In other cases, between the RSW and the tube wall, the attached oblique shock wave AB and the rear shock wave BC (Fig. 1a) occur, and the flow separates from the wall region where it is then concentrated below triple point B in the vicinity of the shock wave (SW) [2]. This phenomenon is called the bifurcation of the reflected shock wave. When an RSW propagates along the smooth tube, at some distance from the endwall the triple-point trajectory corresponds to the case of

Communicated by Harald Kleine.

✉ A. Skilandz  
skilandz.av@gmail.com

<sup>1</sup> A.V. Luikov Heat and Mass Transfer Institute of the National Academy of Sciences of Belarus, Minsk, Belarus

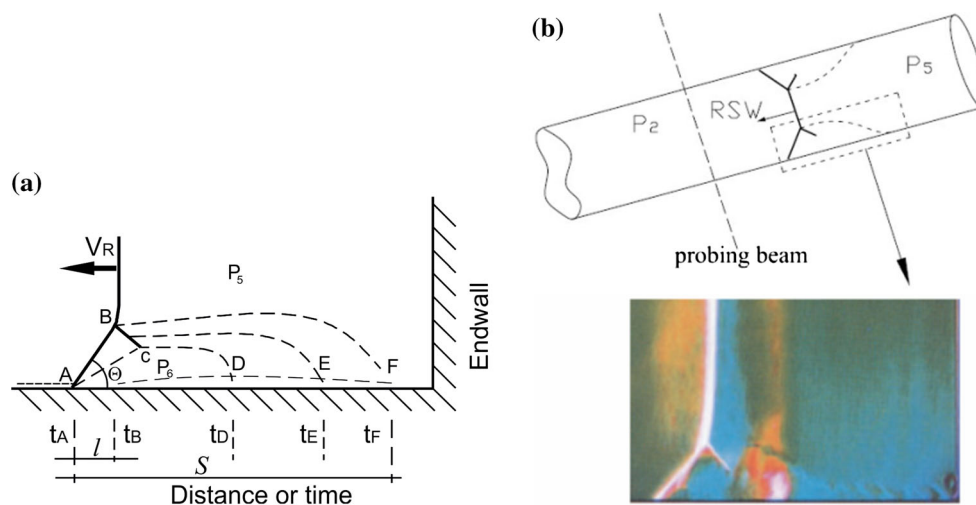


**Fig. 1** Bifurcation structure behind the reflected shock wave (a) and the location of the bifurcation structure in the cylindrical shock tube relative to the probing schlieren beam (b). Schlieren picture was taken from [7]

direct Mach reflection wave configuration. As the distance is increased, the triple-point trajectory is similar to the stationary Mach reflection case [4]. For a rough surface at high Mach numbers [5], no unsteady-to-steady state transition is found, whereas in [6] it is stated that the bifurcation leg stops growing in any case, but the distance prior to the unsteady-to-steady state transition depends on the ISW Mach number, the specific heat ratio, and flow conditions: for example, tube diameter and surface roughness. Usually, the bifurcation phenomenon is studied experimentally and numerically in 2D rectangular channels (Fig. 1a). Figure 1b shows the spatial location of the bifurcation structure in a cylindrical shock tube relative to the probing schlieren beams and the example of color schlieren pictures obtained for a rectangular channel [7].

The analysis of the reasons for the initiation of bifurcation in [2,8] enables one to assume that the bifurcation exists over some range of lower and upper limiting Mach numbers. From [8], it also follows that different theories give conflicting low limiting Mach numbers,  $M_{low}$ , at which bifurcation begins to exist. However, none of the models allows one to explain the experimental values of  $M_{low}$  for different gases. As the models [2,8] are based on different assumptions for gas parameters near the wall, it can be concluded that the bifurcation existence limits are affected by the substantial non-uniformity conditions, at which the gas is near the wall. In such a case, to describe the bifurcation initiation, additional flow parameters along the incident shock wave and the specific heat ratio of a test gas should be taken into consideration.

The bifurcation formation is affected both by the pressure difference between the flow core and the wall region [2] and by the flow interaction at the wall behind the incident shock wave and below the triple point [3,9,10]. The interaction of

the high-intensity RSW with the boundary layer causes a local growth of the boundary layer, and the flow separation since the latter is influenced by increasing the ratio of the pressure behind the shock wave  $p_2$  to the pressure before the shock wave  $p_1$ . When the RSW interacts with the turbulent boundary layer in air, no flow separation occurs if  $p_2/p_1 < 1.8$ . This corresponds to the flow core Mach number  $< 1.3$  [11]. With no flow separation, the RSW–boundary layer interaction does not have a strong influence on the total flow field.

The boundary layer growth is also affected by the ISW Mach number, the boundary layer thickness, and the shape factor [9]. When the reflected shock wave interacts with a laminar boundary layer, a strongly divergent beam of rarefaction waves is formed. This inhibits the formation of a shock wave near the surface. On the contrary, when the reflected shock wave interacts with a turbulent boundary layer, a single shock wave is formed. Some turbulence generation could be used for homogenizing surface conditions due to the enhancement of momentum transfer between internal and external boundary layer regions. In this case, the velocity profile near the wall becomes less sharp, and the boundary layer appears to overcome higher pressure gradient values with no flow separation.

From the above, it cannot be concluded which of the factors has a high priority for the formation and development of the bifurcation structure. So, for these particular cases experimental studies of the RSW interaction with the boundary layer when small-scale turbulence is created artificially are required. It is assumed that such interactions can hinder the formation of large vortices near the wall behind the incident shock wave. The interaction with small-scale turbulence of the boundary layer instead with large vortices or with large density gradients favors the decrease in gas

dynamic fluctuations in the gas behind the bifurcation structure.

This is very important for studies of the chemical kinetics behind a reflected shock wave because the local flow parameters in the shock tube can substantially affect the accuracy of the results [12, 13]. Strong dilution of a reacting mixture with a monoatomic gas can reduce the bifurcation impact on the structure and local flow parameters, but sometimes this does not enable one to solve practical problems, in particular dealing with studies of chemical kinetics in shock tubes with high concentrations of reactants. In addition, when modeling the processes at real flow conditions, it is reasonable to use undiluted gas mixtures. For the sensitive acetylene–air mixture, the experimental approaches of Yamashita and his co-authors [13] showed that mild ignition can exist in shock tube experiments as a consequence of the bifurcation effect. According to the results [13], at the mild ignition behind the reflected shock wave, auto-ignition spots appear mainly along the trajectory of the triple point of the bifurcation structure. Several theoretical models of the bifurcation structure have also suggested that the measurement process is strongly affected by local temperature non-uniformities in the center of vortices that originate within the bifurcation structure below the triple point [14, 15].

To define the extent of the bifurcation influence on kinetic measurements, results of the induction time, one should compare the influence of different parameters of the reflected shock wave bifurcation on local flow characteristics (temperature, concentration, pressure). The objective of the present study is to measure bifurcation structure dynamics and flow parameters in the cylindrical shock tube of different roughnesses when the reflected shock wave interacts with the unsteady boundary layer in air, argon, and a hydrogen–nitrogen mixture. The latter is a representative gas analog of the reactive stoichiometric hydrogen–air mixture. The relevance of our research is in part due to the fact that bifurcation in cylindrical tubes is not widely studied. In addition, our work is important because of the predominant use of cylindrical shock tubes in determining the induction time of reactions in shock tubes, and because of a number of contradictions in the bifurcation theory outlined in this article. Special attention was paid to the influence of small-scale turbulence behind the incident shock wave on overshooting pressures behind the reflected shock wave near the tube wall that originated due to the reflected shock wave–boundary layer interaction. It was assumed that the small-scale turbulence would prevent the occurrence of large vortices during the formation of the boundary layer behind the incident shock wave and decrease amplitudes of pressure and temperature fluctuations in the post-shock flow.

Moreover, we made attempts to stabilize an axisymmetric location and flow parameters of the laminar-to-turbulent transition zone in the boundary layer behind the ISW. We

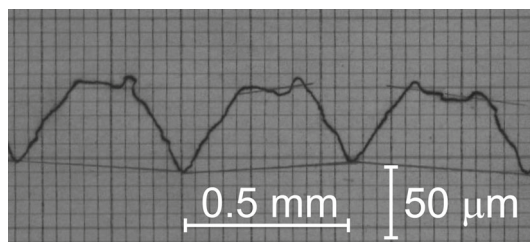


**Fig. 2** Roughness profile of the test section

assumed that the uniformly distributed roughness of the channel would compensate for the axial asymmetry of boundary layer distributions caused by the structural “defects” of the channel and spatial inhomogeneity of the laminar-to-turbulent flow transition zone with respect to the tube perimeter.

## 2 Experimental facility and measurements

Schlieren measurements of the bifurcation structure were taken in a 76-mm-inner-diameter helium-driven shock tube at the deflection of a plane-parallel beam propagating at a small angle to the reflected shock wave plane at 50, 150, and 250 mm from the endwall. Experiments were conducted for a smooth tube with  $Ra = 0.18 \pm 0.04 \mu\text{m}$  and for a rough surface with a profile height of  $60 \pm 5 \mu\text{m}$  ( $Ra = 20 \pm 3 \mu\text{m}$ ) (Fig. 2). In the both cases,  $Ra$  was measured along the tube axis. A roughness height was chosen so that its influence on the flow core would be minor. Based on the results in [16], a roughness height of less than  $100 \mu\text{m}$  should be chosen, since in this case the changes in the flow core and the incident shock wave front will be small. If the roughness height is too small, then its influence on turbulence will manifest itself only at some distance from the roughness element or will not occur at all [11].

The measurements of the oblique shock wave axial projection were similar to those used in [17, 18]. The probing light beams passed through 5-mm-diameter quartz optical windows mounted into the tube wall at the corresponding locations (Fig. 3). The light beam slope angle to the plane of the normal component of the reflected wave was  $3 \times 10^{-3}$  rad. A beam cross section was reduced to 0.55 mm via vertical slots. With regard to the beam width and slope, the method spatial resolution was 0.8 mm. The high sensitivity of the method was provided by the use of long-focus mirrors ( $f \approx 2$  m) and a photomultiplier tube (PMT) as the detecting light sensor. The method yields a systematic error in defining the oblique shock wave axial projection length equal to 0.28 mm. The systematic error was subtracted from all the values measured by the optical system. The optical system allowed simultaneous measurements only at two locations. Therefore, to determine bifurcation parameters at the third location from the endwall, experiments were repeated

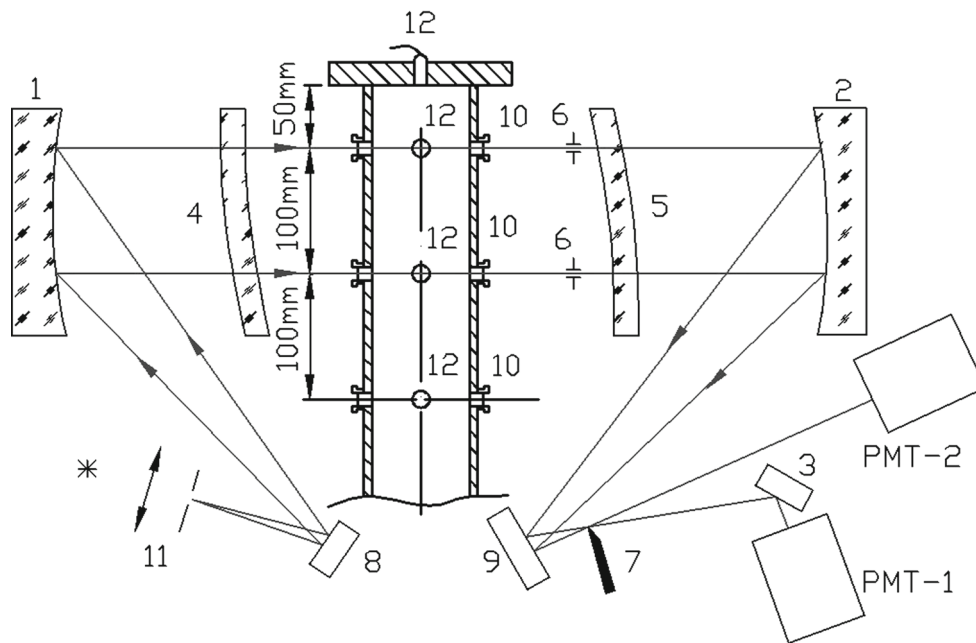


**Fig. 3** Optical setup and the pressure sensor arrangement: 1, 2, 3 mirrors; 4, 5 menisci; 6 0.55-mm-wide vertical slot; 7 knife edge; 8, 9 mirrors; 10 optical windows; 11 vertical slot and illuminating system; 12 pressure sensors

again at the same test and flow conditions. Pressures were measured by piezoelectric sensors mounted into tube wall at distances of 0, 50, 150, and 250 mm from the endwall. The arrangement of pressure sensors and the positions of probing beams are shown in Fig. 3. The intensity of the light, which had passed through the test volume, was recorded using PMT-1 and PMT-2 (Fig. 3). Typical pressure and schlieren PMT records in air and argon are presented in Fig. 4.

As far as the reflected shock wave is moving, the slope angle of the oblique shock wave remains constant, but depends on the incident shock wave Mach number. Knowing the length of the oblique shock wave projection onto the shock tube surface or otherwise the axial projection of the oblique shock wave, it is possible to calculate the triple-point height and sizes of other bifurcation elements.

We measured the time difference between the positions of flow separation point  $t_A$  and normal reflected shock wave  $t_B$ , that is,  $\Delta t_{BA}$  (Figs. 1, 4). The  $t_A$  value was measured in the middle of the section of a sharply increasing pressure sensor signal since the sensor had a finite width and the pressure at the shock wave front changed intermittently. The  $t_B$  value was consistent with the peak of the schlieren signal. The axial projection  $l$  of the oblique shock wave was calculated as the product  $\Delta t_{BA} V_R$ , where  $V_R$  is the reflected shock wave velocity. In such  $l$  measurements, at a distance  $x$  up to the endwall, the axial projection of the oblique shock wave was found at the moment when the front of the normal component of the RSW was at the distance  $(x - l)$  from the endwall.

To assess experimental errors, the parametric uncertainties for maximum and minimum Mach numbers were calculated.

The uncertainties of the incident wave velocity and Mach number  $M = 1.27$  in air were 1.1%, of the initial pressure—0.4%, of the length of the oblique shock wave projection—5.5% at a distance of 50 mm, and 4% at distances of 150 and 250 mm. For  $M = 3.4$ , the error of the velocity was 1.2%, that of the initial pressure—0.6%, that of the length of the oblique shock wave projection—1.6% at a distance of 50 mm, and 1.3% at distances of 150 and 250 mm. Measurements of the hydrogen–nitrogen mixture were taken with the same accuracy. In all experiments, the initial pressure error did not exceed 0.8%. The initial temperature error was 0.2 K, i.e., 0.7%.

In argon experiments, the errors of incident shock wave velocity and Mach number are  $< 1.1\%$ , and the error of initial pressure— $< 0.6\%$ . The maximum error of the length of the oblique shock wave projection is 5% at a distance of 50 mm and is 4.7% at distances of 150 and 250 mm, respectively.

Studies are performed for the following post-shock flow conditions: for argon  $T_5 = 670\text{--}2900$  K ( $\varepsilon < 2\%$ ),  $P_5 = 0.37\text{--}1.65$  MPa ( $\varepsilon < 3.8\%$ ),  $\rho_5 = 2.79 \pm 0.14$  kg/m<sup>3</sup> ( $\varepsilon < 2\%$ ),  $\gamma_2 = \gamma_5 = 1.667$ ,  $M = 1.49\text{--}3.50$ ; for air  $T_5 = 480\text{--}1740$  K ( $\varepsilon < 2\%$ ),  $P_5 = 0.395\text{--}1.419$  MPa ( $\varepsilon < 5.5\%$ ),  $\rho_5 = 2.80 \pm 0.13$  kg/m<sup>3</sup> ( $\varepsilon < 4\%$ ),  $\gamma_2 = 1.334\text{--}1.394$ ,  $\gamma_5 = 1.303\text{--}1.386$ ,  $M = 1.50\text{--}3.60$  ( $\varepsilon < 1.2\%$ ); for a representative hydrogen–nitrogen mixture  $0.704$  N<sub>2</sub>+ $0.296$  H<sub>2</sub> at  $M = 1.70\text{--}3.26$ ,  $T_5 = 609\text{--}1496$  K ( $\varepsilon < 2\%$ ),  $P_5 = 0.72\text{--}1.59$  MPa ( $\varepsilon < 5.0\%$ ),  $\rho_5 = 2.81 \pm 0.12$  kg/m<sup>3</sup> ( $\varepsilon < 4\%$ ),  $\gamma_2 = 1.362\text{--}1.395$ ,  $\gamma_5 = 1.323\text{--}1.388$ .

The errors of the parameters  $T_5$ ,  $P_5$  are defined through the variations of initial pressure, shock wave velocity, and

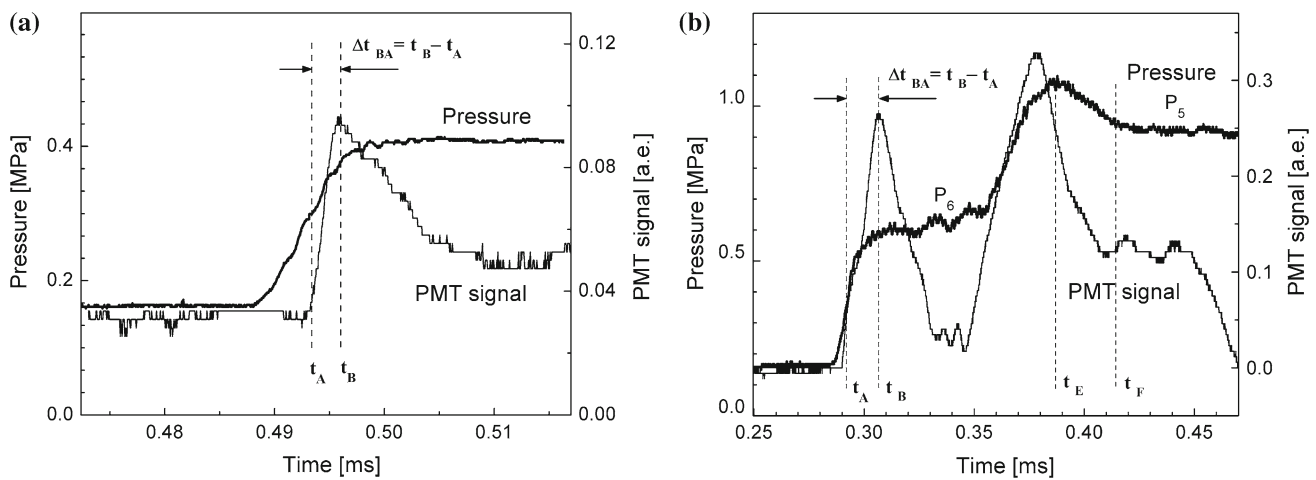


**Fig. 4** Pressure and PMT records of the schlieren intensity variation in argon (a) at  $M = 3.6$  and in air (b) at  $M = 3.8$ . Distance of 50 mm from the endwall

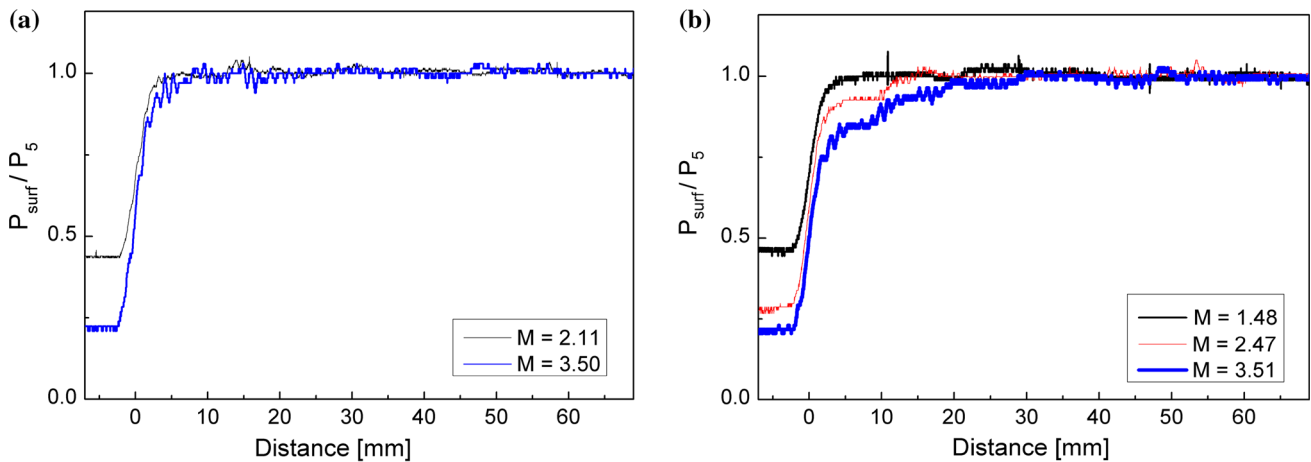


**Fig. 5** Pressure distributions behind the reflected shock wave in argon versus the distance from a point 50 mm from the endwall at different ISW Mach numbers: **a** smooth tube; **b** rough tube

temperature values using CHEMKIN database and do not incorporate the error of the  $\gamma$  approximation by the polynomial  $\gamma(T)$  and also the error due to the discreteness of the computational method used in the software. The most substantial contribution to the calculated error is made by the error (1%) of defining the incident shock wave velocity caused by changes in the velocity of the incident shock wave as far as it approaches the endwall.

### 3 Results

#### 3.1 Argon

As the Mach number is increased, a minor pressure growth can be observed after the shock wave has passed the measurement cross sections (Fig. 5). Schlieren records are specific both for the position of a signal maximum with respect to the

start of the signal growth and for the changes in the signal shape. This can be indicative both of the transient processes in the boundary layer and of the bifurcation structure development. For the smooth tube in argon at a distance of 50 mm, the axial projection  $l$  of the oblique shock wave remains constant with increasing Mach number (Fig. 6). As the distance to the endwall is increased,  $l$  grows. This can point to the fact that there occurs a laminar-to-turbulent flow transition in the boundary layer that develops at a certain distance upstream of the endwall. If the laminar-to-turbulent flow transition in the boundary layer is assumed to occur at  $\text{Re}_{\text{BL}} = 10^6$  [19], then over the ISW Mach number and density ranges investigated, the distance from the incident shock wave to the laminar-to-turbulent flow transition zone is within 72–90 mm for the smooth shock tube. When the boundary layer development is enhanced due to the surface roughness,  $l$  grows with Mach number even at a distance of 50 mm (Fig. 6). For the rough tube at 150 and 250 mm, the  $l(M)$  data almost coin-

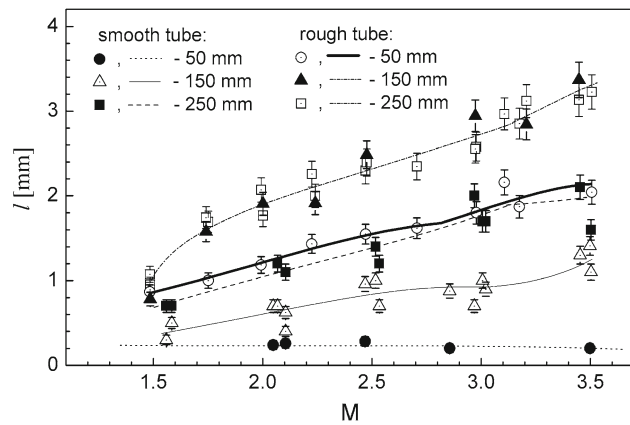


**Fig. 6** Axial projection  $l$  of the oblique shock wave versus incident shock wave Mach number in argon at different distances from the endwall, experimental data and trend lines

cide. So, the unsteady-to-steady state transition is reached for distances less than 150 mm. In [3], the bifurcation is assumed to exist in argon and according to the calculations the axial projection of the oblique shock wave must attain a constant value of 1.4 mm as the distance to the endwall is increased at  $M = 2.0$ . In our experiments, for the smooth tube the steady-state regime is not reached for the studied range of ISW Mach numbers, whereas for the rough tube, at distances of 150 mm the steady-state regime is attained.

At  $M = 2.0$ , the length of the oblique shock wave axial projection for the smooth tube is equal to  $l \approx 1$  mm and at  $M = 3.1$ ,  $l \approx 1.8$  mm, respectively. As shown in Fig. 6, for the rough tube at  $M = 1.48$ , the  $l$  values are almost equal for all measurement cross sections. Based on the  $l(M)$  data, it can be assumed that bifurcation is absent at  $M = 1.48$  even when the boundary layer is enhanced due to the wall roughness. This does not contradict Mark’s model consequence that the bifurcation exists in argon at the Mach number  $> 1.57$ .

### 3.2 Air

As the bifurcation structure moves together with the reflected shock wave, the local time of the pressure distribution measured by pressure sensors is assumed to be identical to that along the tube wall behind the RSW. At different ISW Mach numbers, the local signal time was multiplied by the reflected shock wave velocity  $V_R$  to obtain a distance behind the flow separation point A (Fig. 1). The measured pressure distributions along the wall behind the oblique shock wave in air are shown in Fig. 7. Records are normalized to the pressure  $P_5$  behind the reflected shock wave attained after the passage of the bifurcation structure through the measurement cross section. Such a representation of the flow structure enables one to estimate the excess of the pressure (overshoot pressure) at the point where the flow stagnation line intersects

the tube wall (point E, Fig. 1) over  $P_5$  near the endwall. For the rough tube at  $M > 3$  it seems that the flow is re-attached between A and D, and the pressure profile characteristic for double Mach reflection is formed at lower Mach numbers. For the rough surface, the overshoot pressure caused by bifurcation region vortices [15, 16] is enhanced. For  $M = 3.5$ , the pressure excess over the pressure  $P_5$  at point E attains the value that is by a factor of 2 more than that for the smooth tube. Hence, for the roughness used in experiments it was impossible to attain the reduction in the overshoot pressure by artificially initiating small-scale turbulence.

The formation of the bifurcation structure is associated with an excess of the pressure  $P_5$  over the wall pressure  $P_6$  behind the oblique shock wave and is detailed in [2]. The condition for  $P_5 > P_6$  is taken as the bifurcation initiation [2, 8]. Figure 8 illustrates the curves for the ratio of the pressure  $P_6$  to the pressure  $P_5$  to be attained over the same cross section at the distances of 100–150 mm behind the RSW. At high Mach numbers or at a high turbulence level, the boundary layer can separate behind the oblique shock wave. The pressure  $P_6$  is measured at a time instant corresponding to a distance of 3 mm behind the front of the oblique shock wave, i.e., at the moment when flow separation point A (Fig. 1) has fully passed the pressure sensor.

Although Mark’s model assumes that the reflected shock wave interacts with the laminar boundary layer near the flat surface, the  $P_6/P_5$  data obtained in our experiments and their theoretical  $P_{BL}/P_5$  values were used for comparison. The  $P_{BL}$  value is calculated by

$$M_{BL} = \frac{2(\gamma - 1)M^2 + 3 - \gamma}{(\gamma + 1)M};$$

$$M_{BL} < 1 : \frac{P_{BL}}{P_2} = \left[ 1 + \frac{\gamma - 1}{2} M_{BL}^2 \right]^{\gamma/(\gamma-1)};$$

$$M_{BL} > 1 : \frac{P_{BL}}{P_2} = \left[ \frac{\gamma + 1}{2} M_{BL}^2 \right]^{\gamma/(\gamma-1)} \cdot \left[ \frac{2\gamma}{\gamma + 1} M_{BL}^2 - \frac{\gamma - 1}{\gamma + 1} \right]^{1/(1-\gamma)}, \quad (1)$$

where  $M_{BL}$  is the boundary layer Mach number;  $M$  is the ISW Mach number;  $P_2$  is the pressure behind the front of the incident shock wave; and  $\gamma$  is the specific heat ratio.  $P_2$  values are determined from our experiments. In [5], for  $M = 4-9$  the specific heat ratio  $\gamma_2$  behind the ISW was used instead of the specific heat ratio  $\gamma_1$  at the initial conditions.

Having compared the results of both cases, it was concluded that in our case, the use of the calculated  $\gamma_1$  values yielded the results closer to the experimental ones. This specified the choice of  $\gamma_1$  values for calculation both of  $P_{BL}$  and of slope angles of the oblique shock wave to the tube wall  $\theta$  when the pressure behind the oblique shock wave near the flow separation point was equal to  $P_6$  and  $P_{BL}$  values.

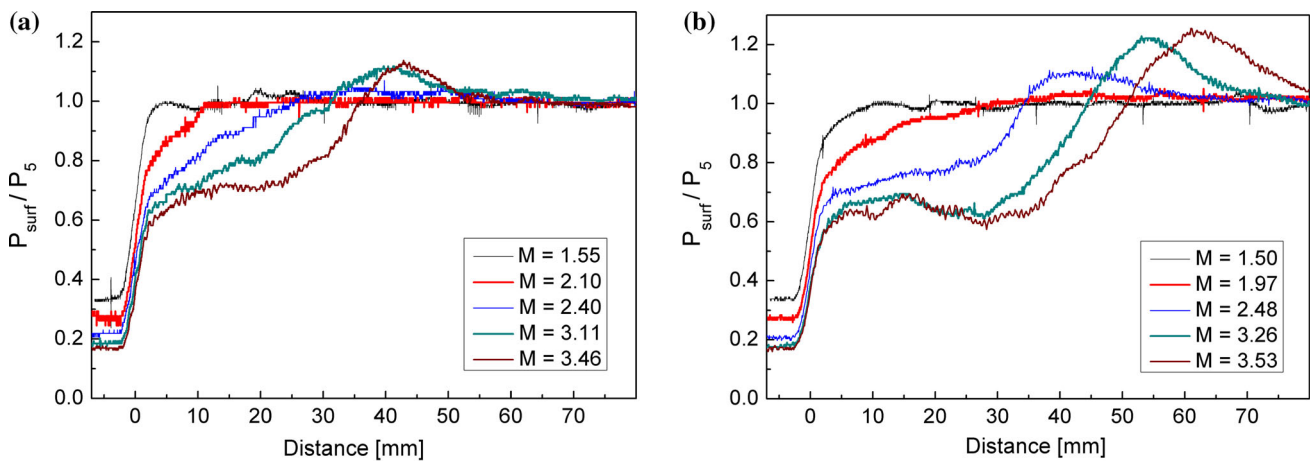


**Fig. 7** Pressure distributions behind the oblique shock wave in air versus the distance at 50 mm from the endwall at different ISW Mach numbers: **a** smooth tube; **b** rough tube

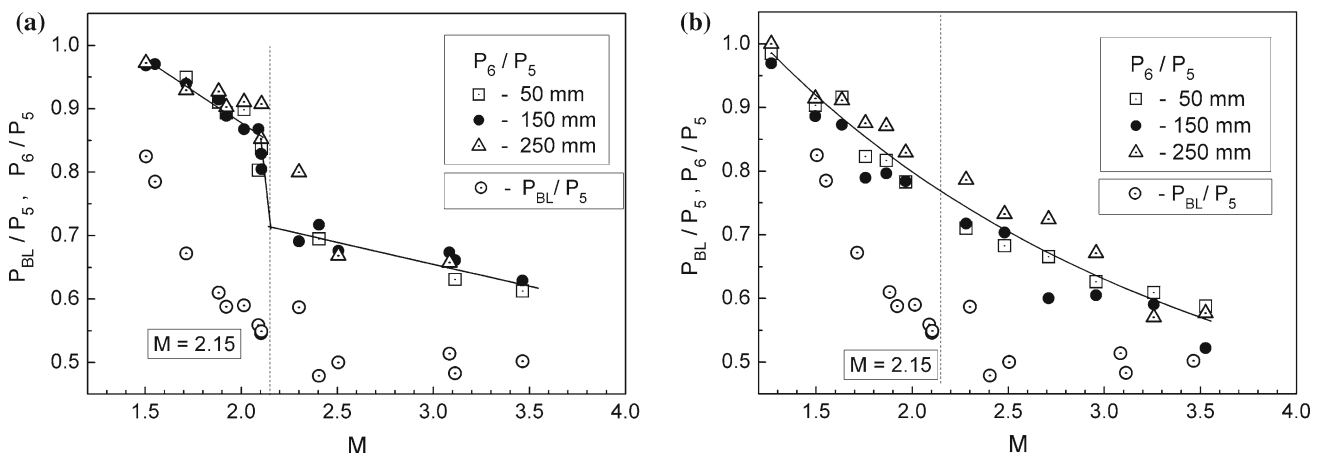


**Fig. 8** Ratio of the pressure  $P_6$  behind the oblique shock wave to the flow core pressure  $P_5$  versus ISW Mach number: **a** smooth tube; **b** rough tube

From Fig. 8 it is seen that the approximating curve for  $P_6/P_5$  for the smooth surface has a bend at the incident shock wave Mach number equal to 2.15, at which the flow in the boundary layer starts to be sonic. At  $M < 2.15$ , both experimental and theoretical approximating curves for  $P_6/P_5$  are strongly different; the experimental data points for the smooth tube lie substantially above. At  $M > 2.15$ , the approximating curves for  $P_6/P_5$  almost coincide, but the rough tube data are characterized by a more considerable scatter. For the rough tube at  $M < 2.15$ , the pressure  $P_6$  becomes lower, approaching the theoretical boundary layer pressure  $P_{BL}$ .

To calculate the slope angles of the oblique shock wave to the tube wall  $\theta$ , the following expression is used

$$M_R^2 \sin^2(\theta) = \frac{(\gamma + 1) \frac{P_{BL}}{P_2} + \gamma - 1}{2\gamma}, \quad (2)$$

where  $M_R$  is the reflected shock wave Mach number [2, 18]. For comparison, the predicted and experimental  $P_6$  values

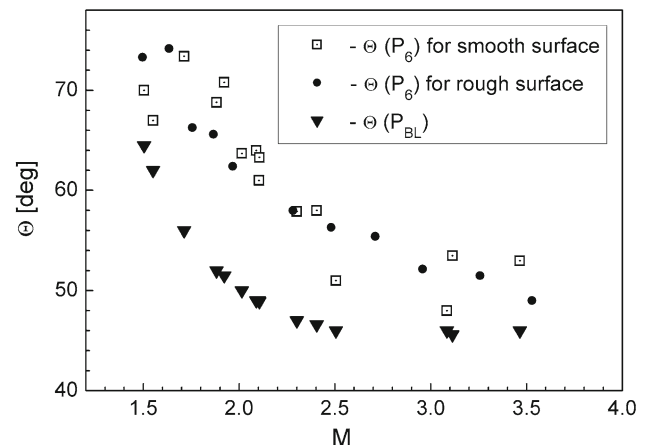


**Fig. 9** Slope angle of the oblique shock wave to the smooth tube wall versus ISW Mach number

are used as  $P_{BL}$ . The calculation results are demonstrated in Fig. 9.

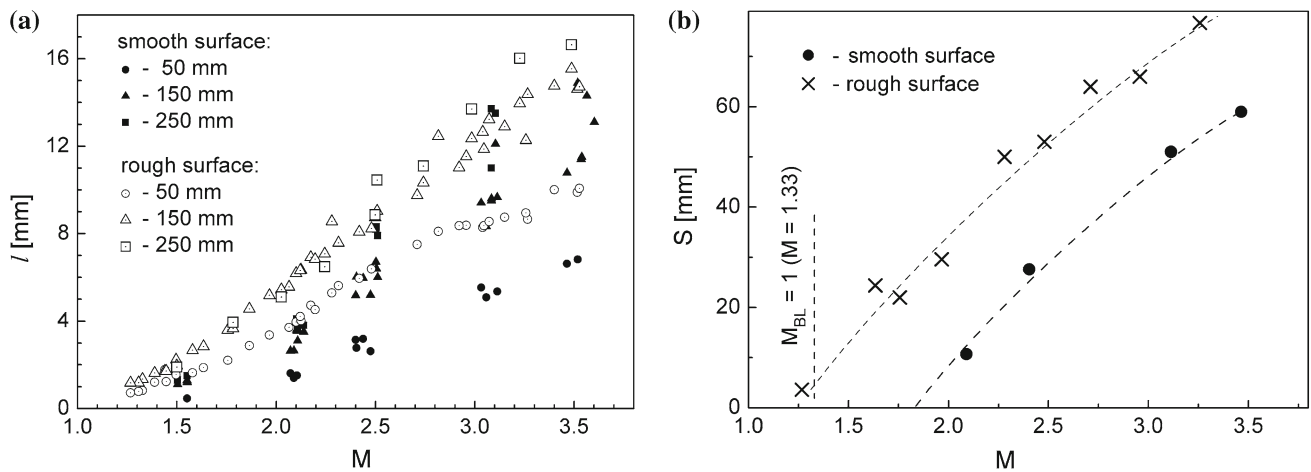


**Fig. 10** Axial projection  $l$  of the oblique shock wave versus incident shock wave Mach number for air (a); axial flow distance  $S$  versus incident shock wave Mach number at 50 mm from the endwall (b) (see Fig. 1)

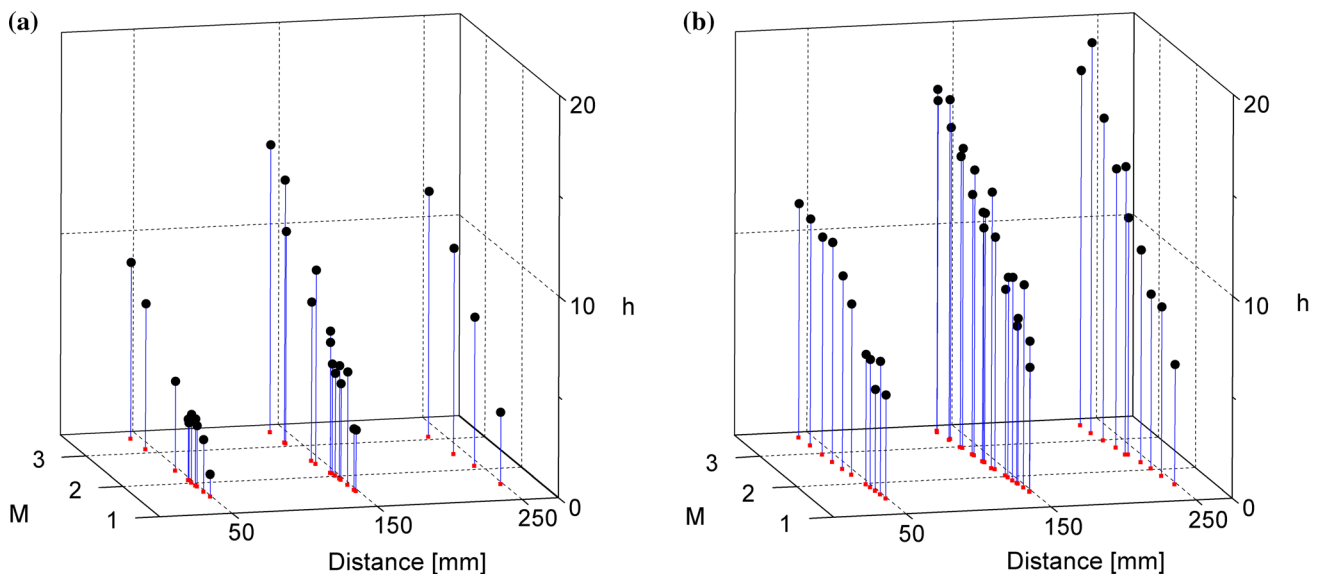


**Fig. 11** Triple-point height  $h$  versus incident shock wave Mach number and distance for air: **a** smooth tube; **b** rough tube

For the smooth tube in air, the  $l$  value grows with increasing Mach number and distance to the endwall (Fig. 10a). For the rough surface at a distance between 150 and 250 mm, the steady-state bifurcation regime is achieved. A growth of the axial projection of the oblique shock wave is not observed, at least, for the Mach numbers more than 2.7. For the smooth tube, the  $l$  attains similar values for the rough surface at Mach numbers more than 2.5 and at a distance of 250 mm to the endwall. Thus, at a distance larger than 150 mm to the endwall and at Mach numbers more than 2.5 there exists a bifurcation regime common for smooth and rough tubes.

The  $l$  growth with increasing Mach number remains close to the linear one for each distance to the endwall (Fig. 10a). The bifurcation structure is characterized by the linear  $l$  growth with increasing distance to the endwall to attain some

value. After this, the steady-state regime of the bifurcation is achieved, and its structure size depends on the boundary layer thickness [5]. The  $l$  increasing with distance for the smooth tube does not contradict the results [5] for nitrogen at higher Mach numbers. However, in [5], the steady-state regime is not found at a certain distance when the roughness profile height is 1.2 mm. In our case, for the rough tube the distance at which the bifurcation structure size increases with distance is smaller than that for the smooth tube. The dependence of the distance to achieve the steady-state regime on the tube roughness and diameter is outlined elsewhere in [6].

The axial projection of the oblique shock wave linearly increases with distance that it has passed along the motionless entropy layer to 300–400 heights of the laminar boundary layer for the cylindrical channel [3]. In our case, according



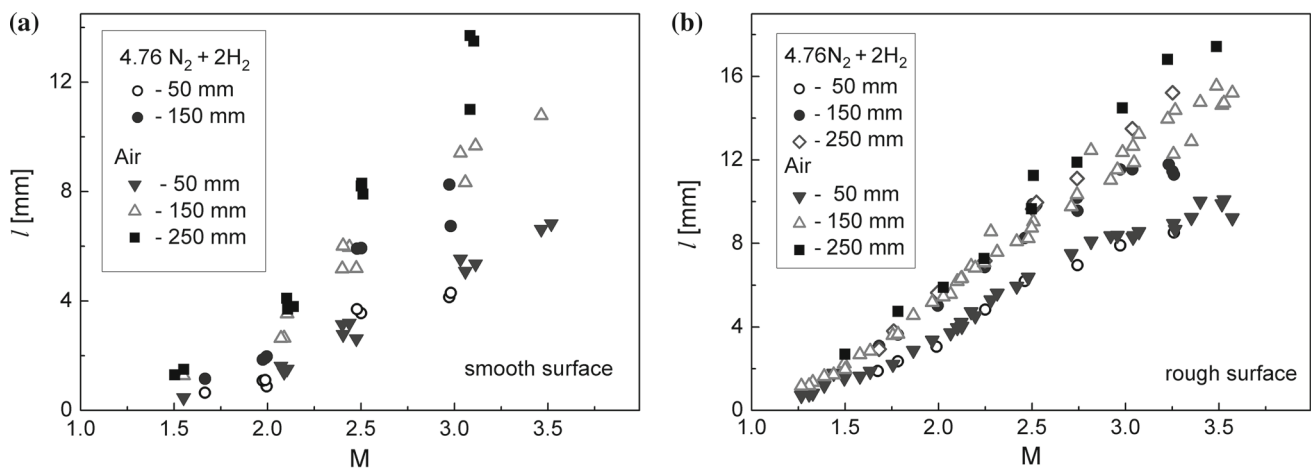


**Fig. 12** Axial projection length  $l$  of the oblique shock wave versus incident shock wave Mach number for air and hydrogen–nitrogen mixture: **a** smooth tube; **b** rough tube

to the calculations for  $M = 1.33$  in air, the laminar boundary layer thickness is 0.6 mm. This is consistent with a distance of 180 mm behind the incident shock wave. The reflected shock wave reaches this location at a distance of 76 mm upstream of the endwall. As a result, we cannot observe a linear growth of the bifurcation structure with distance between 50 and 150 mm to the endwall.

The  $l$  scatter with increasing distance is caused by the growth of the wave front deviation from the axial symmetry that originates due to both the channel geometry error and a random distance from the incident shock wave to a laminar-to-turbulent boundary layer transition zone. For the Mach number ranges, for which the  $l(M)$  dependence is most close to the linear one, the mean deviation of the obtained data from the approximating line has been calculated. It has appeared that the scatter of the results for the smooth tube is by a factor of 1.5 more than that for the rough tube. The same effect is also observed for argon. From this it follows that, indeed, the wall roughness can be used for stabilizing the boundary layer development behind incident and, consequently, reflected shock waves.

Figure 10b shows the axial distance ( $S$ ) between flow separation point A (Fig. 1) and the end of the region of flow disturbance caused by bifurcation near the wall measured at 50 mm from the endwall (Fig. 4b, time  $t_F$ ). The bifurcation arises for the Mach number, at which the curves in Fig. 10b intersect the abscissa axis. Mark's theory predicts the bifurcation existence in air over the Mach number range 1.33–6.45 [2]. In our experiments, we did not study the upper limit of this range. From Fig. 10b, it can be concluded that small roughness can provide the condition when the experimental lower bifurcation limit becomes closer to its theoretical value. Probably, this means that the gas in the boundary layer for the rough tube has a temperature that is almost the same as the wall temperature since the roughness enhances heat

transfer. It is known that the boundary layer separation can affect the bifurcation development [4]. The bifurcation limit depends not only on the incident shock wave Mach number, but also on the boundary layer type. It can be assumed that at  $M = 1.3$  for the rough tube the bifurcation cannot arise or can slowly increase up to  $M \approx 1.8$ . Over the Mach number range 2.0–2.75, the  $S$ -to- $l$  ratio for rough and smooth tubes coincides for the same  $l$  values but differs for the same Mach numbers. Hence, the nature of the impact of small-scale turbulence for the selected roughness mainly does not differ from that for the smooth surface, since this does not change the size ratio of bifurcation structure parameters.

In [2], at a distance of 54 mm for  $M = 2.15$ ,  $p_1 = 6.08$  kPa in air the triple-point height was 5.2 mm. At a slope angle of the oblique shock wave equal to  $48^\circ$ , the axial projection of the oblique shock wave was 4.4 mm. For our experimental conditions, such a value was attained only at  $M = 2.25$  at a distance of 50 mm for the rough tube. This can be a consequence of the influence of increased turbulence being initiated at the corners of the rectangular shock tube [2].

To describe the triple configuration, besides the pressure  $P_6$  it is necessary to know the triple-point trajectory and the reflected shock wave Mach number [8]. It is impossible to directly measure the triple-point height  $h$  in the cylindrical channel using our experimental method. However,  $h$  values can be calculated as  $l \tan(\Theta)$ . The triple-point trajectory can then be obtained as the function  $h(l, \Theta, x)$  where  $x$  is the distance to the endwall. The results of  $h$  calculations are represented in Fig. 11. The distance in this figure is the distance from the endwall to the normal reflected shock wave calculated by the formula  $x = (50 - l)$ , or  $x = (150 - l)$ , or  $x = (250 - l)$  mm for each measurement cross section, respectively.

### 3.3 Bifurcation in a representative gas analog of the stoichiometric hydrogen–air mixture

Figure 12 shows the results of the axial projection  $l$  of the oblique shock wave in the  $0.704\text{N}_2 + 0.296\text{H}_2$  mixture, that is the non-reacting gas analog of a stoichiometric hydrogen–air mixture. The use of the non-reacting gas analog enabled one to exclude the influence of chemical reactions on measurement results, as well as to reduce the influence of the gas luminosity on schlieren intensity variations when recording a light beam passing through the test volume. Similar specific heat ratios (for air  $\gamma = 1.40$ , hydrogen  $\gamma = 1.41$ , nitrogen  $\gamma = 1.40$ ), molecular weights, and dynamic viscosities are a criterion for choosing the gas analog for RSW bifurcation studies. From Fig. 12 it follows that the bifurcation behavior in the  $0.704\text{N}_2 + 0.296\text{H}_2$  mixture for smooth and rough tubes exhibits a close agreement with measurement results for air behind the reflected shock wave. This means that these results are also applicable for estimation of the bifurcation structures in other fuel–air mixtures with a large air amount.

## 4 Conclusions

The results of the present study show that small roughness exerts a stabilizing influence on the bifurcation structure. Hence, when small roughness is used, the flow is stabilized behind the incident shock wave since the bifurcation arises due to the reflected shock wave–boundary layer interaction. The availability of small-scale turbulence due to the rough surface for  $Ra = 20\ \mu\text{m}$  at the incident shock wave Mach number equal to 3.5 in air increases the overshoot pressure behind the reflected shock wave by a factor of 2 and the oblique shock wave axial projection length by a factor of 1.5 at a distance of 50 mm to the endwall. Thus, not all stabilization characteristics are improved for a wall roughness of  $20\ \mu\text{m}$   $Ra$ .

We revealed that the lower bifurcation limit measured in the rough tube in air correlated well with the predictions of Mark's theory. The values of the axial projection of the oblique shock wave obtained for the rough cylindrical shock tube are close to those in [2] for the smooth rectangular tube.

For the rough tube, the steady-state bifurcation regime is attained at a distance between 50 and 150 mm and the axial projection of the oblique shock does not grow, at least, to a Mach number of more than 2.7 for air and over the entire argon range. For the smooth tube, the axial projection of the oblique shock wave is the same as for the rough tube at Mach numbers more than 2.5 at a distance of 250 mm to the endwall. Thus, the bifurcation regime common for smooth and rough surfaces exists at a distance of more than 150 mm from the endwall and at a Mach number of more than 2.5. This regime

does not depend on bifurcation structure parameters that are observed at a smaller distance.

Our studies show that our results concerning the bifurcation structure size for air can be used to assess the bifurcation parameters of the reflected shock wave in the  $0.704\text{N}_2 + 0.296\text{H}_2$  mixture, that is the non-reacting gas analog of the stoichiometric hydrogen–air mixture. This makes it possible to assume the applicability of the obtained results for assessment of bifurcation parameters in mixtures having large air amounts.

## References

1. Hadjadj, A., Dussauge, J.P.: Shock wave boundary layer interaction. *Shock Waves* **19**, 449–452 (2009). doi:[10.1007/s00193-009-0238-2](https://doi.org/10.1007/s00193-009-0238-2)
2. Mark, H.: The interaction of a reflected shock wave with the boundary layer in a shock tube. NASA TM-1418 (1958)
3. Starikovskii, A.: Nonlinear waves and energy exchange in reacting systems. Phd. thesis, MFTI, Moscow (1999) (in Russian)
4. Ben-Dor, G., Takayama, K.: The phenomena of shock wave reflection—a review of unsolved problems and future research needs. *Shock Wave* **2**(4), 211–223 (1992). doi:[10.1007/BF01414757](https://doi.org/10.1007/BF01414757)
5. Taylor, J.R., Hornung, H.G.: Real gas and wall roughness effects on the bifurcation of the shock reflected from the endwall of a tube. In: Treanor, C.E., Hall, J.G. (eds.) *Shock Tubes and Waves, Proceedings of 13th International Symposium on Shock Tubes and Waves*, pp. 262–270. State University of New York Press, Albany, New York (1981)
6. Bazhenova, T.V.: *Shock Waves in Real Gases*. NASA Technical Translation, F-585, Washington, D.C. 20546 (1969)
7. Kleine H., Lyakhov V.N., Gvozdeva L.G., Grönig, H.: Bifurcation of a reflected shock wave in a shock tube. In: Takayama K. (eds) *Shock Waves, Proceedings of the 18th International Symposium on Shock Waves*, pp. 261–266. Springer, Berlin (1992). doi:[10.1007/978-3-642-77648-9\\_36](https://doi.org/10.1007/978-3-642-77648-9_36)
8. Fokeev, V.P., Abid, S., Dupré, G., Vaslier, V., Paillard, C.: Domains of existence of the bifurcation of a reflected shock wave in cylindrical channels. In: Brun, R., Dumitrescu, L.Z. (eds.) *Shock Waves @ Marseille I. Proceedings of the 19th International Symposium on Shock Waves*, 26–30 July 1993, pp. 145–150. Marseille, France (1993). doi:[10.1007/978-3-642-79532-9\\_23](https://doi.org/10.1007/978-3-642-79532-9_23)
9. Couldrick, J.S.: A study of swept and unswept normal shock wave/turbulent boundary layer interaction and control by piezoelectric flap actuation. PhD Thesis, University of New South Wales, Australia (2006)
10. Bulovich, S.V., Vikolayner, V.E., Zverintsev, S.V., Petrov, R.L.: Numerical simulation of the interaction between reflected shock wave and near-wall boundary layer. *Tech. Phys. Lett.* **33**(2), 173–175 (2007). doi:[10.1134/S1063785007020241](https://doi.org/10.1134/S1063785007020241)
11. Schlichting, H.: *Boundary-Layer Theory*, 6th edn. McGraw-Hill, New-York (1968)
12. Penyazkov, O.G., Ragotner, K.A., Shabunya, S.I., Martynenko, V.V.: High-temperature ignition of hydrogen–air mixture at high pressures behind reflected shock wave. *Nonequilibrium Processes in Combustion and Plasma Based Technologies*, International Workshop, August 21–26, Minsk, Belarus (2004)
13. Yamashita, H., Kasahara, J., Sugiyama, Y., Matsuo, A.: Visualization study of ignition modes behind bifurcated-reflected shock

- waves. *Combust. Flame* **159**(9), 2954–2966 (2012). doi:[10.1016/j.combustflame.2012.05.009](https://doi.org/10.1016/j.combustflame.2012.05.009)
14. Daru, V., Tenaud, C.: Numerical simulation of the viscous shock tube problem by using a high resolution monotonicity-preserving scheme. *Comput. Fluids* **38**, 664–676 (2009). doi:[10.1016/j.compfluid.2008.06.008](https://doi.org/10.1016/j.compfluid.2008.06.008)
  15. Daru, V., Tenaud, C.: Evaluation of TVD high resolution scheme for unsteady viscous shocked flows. *Comput. Fluids* **30**, 89–113 (2001). doi:[10.1016/S0045-7930\(00\)00006-2](https://doi.org/10.1016/S0045-7930(00)00006-2)
  16. Duff, R.E.: The interaction of plane shock waves and rough surfaces. *J. Appl. Phys* **23**(12), 1373–1379 (1952). doi:[10.1063/1.1702077](https://doi.org/10.1063/1.1702077)
  17. Soloukhin, R.I.: *Shock Waves and Detonations in Gases*. Mono Book Corp, Baltimore (1966)
  18. Petersen, E.L., Hanson, R.K.: Measurement of reflected-shock bifurcation over a wide gas composition and pressure range. *Shock Waves* **15**, 333–340 (2006). doi:[10.1007/s00193-006-0032-3](https://doi.org/10.1007/s00193-006-0032-3)
  19. Korobeinikov, V.P.: *Unsteady Interaction of Shock and Detonation Waves in Gases*. Hemisphere Publishing Corp, New York (1989)